Sodium Alginate/Chitosan/Activated Carbon Composite Hydrogel for Cyanobacterial Inhibition: RSM Optimization and Sustained Release Performance

Dongmei Jiang and Yingjun Wang *

Posted Date: 30 April 2026

doi: 10.20944/preprints202604.2211.v1

Keywords: citrus peel; algal inhibition; activated carbon; gel microspheres; response surface methodology

 doi:10.20944/preprints202604.2211.v1

Article

Sodium Alginate/Chitosan/Activated Carbon Composite Hydrogel for Cyanobacterial Inhibition: RSM Optimization and Sustained Release Performance

Dongmei Jiang and Yingjun Wang *

College of Environment, Sichuan Agricultural University, Chengdu 611130, China

* Correspondence: wangyingjun@sicau.edu.cn

Abstract

This study presents a sodium alginate/chitosan/activated carbon (SA/CS/AC) gel microspheres loaded with citrus peel allelochemicals for continuous inhibition of *Microcystis aeruginosa* by controlled release. Preparation parameters were optimized via response surface methodology (RSM) for improved algal inhibition, yielding an optimal formulation: 1.97% SA, 0.76% CS, 0.31% AC. The optimized gel microspheres showed a 7-day inhibition rate of 85.17 ± 2.49%, consistent with the predicted 85.29%. Characterization revealed that AC enriched the gel's porous structure and surface functionality, increasing allelochemical adsorption sites, enhancing loading efficiency, and sustaining long-term release with a 25-day cumulative release of 70%. Algal inhibition declined slightly from day 7 to 30 due to allelochemical depletion but remained 76.27%, versus 30.58% for the blank SA/CS/AC carrier and 52.81% for the allelochemical-loaded SA/CS gel microspheres. AC thus synergistically strengthens algal inhibition by elevating allelochemical loading and prolonging activity, providing a feasible strategy for sustainable cyanobacterial bloom control.

Keywords: citrus peel; algal inhibition; activated carbon; gel microspheres; response surface methodology

1. Introduction

In recent years, the loads of agricultural non-point source pollution and urban anthropogenic pollution have remained at high levels. Frequent excessive proliferation of cyanobacteria has been caused by water eutrophication and climate change. Among them, cyanobacterial blooms dominated by *Microcystis aeruginosa* [1] not only lead to water quality deterioration, destroy the aquatic ecological balance and affect fisheries and drinking water safety, but also release microcystins, which pose a serious threat to human health through the food chain [2,3]. Traditional physical and chemical algal control methods are limited by high cost and the risk of secondary pollution [4], which can hardly meet the requirements of green and long-term remediation. In contrast, plant allelochemical-based algal inhibition technology has gradually emerged as one of the most concerned research directions in green algae control due to its advantages of wide availability, biodegradability, low non-target impact, and low treatment cost [5].

Plant-derived allelochemicals are natural secondary metabolites that can effectively inhibit algal growth after being released into the environment [6]. Among them, phenolic compounds, particularly phenolic acids and flavonoids, become the focus of green algal inhibition research due to their wide distribution and remarkable algicidal activity [7]. Cao et al [8] demonstrated that phenolic compounds in rhubarb extracts possess significant allelopathic activity, which can directly damage the cell membrane structure of algae, resulting in cellular rupture and death. In addition to tissues from terrestrial and aquatic plants, various agricultural by-products such as fruit peels have also been verified to be rich in allelochemicals [9]. Relevant research has shown that citrus peels are

 doi:10.20944/preprints202604.2211.v1

rich in allelochemicals, particularly flavonoids and phenolic acids, with total phenolic contents ranging from 16 to 50 mg GAE/g DW [10]—substantially higher than the polyphenol levels of agricultural by-products including straw [11], rice husks [12], and forage [13] (1–20 mg GAE/g DW). Moreover, its aqueous extract exhibits a 7-day inhibition rate of up to 90% against *Microcystis aeruginosa* [14], making it an ideal raw material for the development of natural algicides. However, natural allelochemicals generally exhibit inherent drawbacks such as poor stability, high susceptibility to photolysis and oxidation, and short effective duration [15], which greatly restrict their practical applications. The construction of controlled-release systems using biocompatible hydrogels as carriers can effectively overcome the above bottlenecks, prolong the action period of allelochemicals, and enhance the long-term algal inhibition efficiency [16], representing an important direction for the development of green and long-lasting algicides.

Hydrogels, as polymer carriers with a three-dimensional network structure, show unique advantages in the loading and sustained release of allelochemicals, which can effectively improve the stability of allelochemicals and prolong the algal inhibition duration [17]. Among various gel carriers, sodium alginate (SA) and chitosan (CS) are two typical natural polymers with outstanding advantages including non-toxicity, good biocompatibility, and biodegradability [18,19]. An interpenetrating network structure can be constructed between them via electrostatic interactions, and SA is capable of ionic crosslinking under the induction of divalent cations such as Ca^{2+}, ultimately forming a structurally stable three-dimensional network hydrogel [20,21]. SA/CS hydrogels have emerged as ideal carriers for allelochemical loading owing to their biocompatibility and sustained-release properties. Ni [22] et al. encapsulated artemisinin in SA/CS hydrogels, extending the algae-inhibiting period to over 40 days, which confirms the application potential of such carriers in long-acting algae inhibition.

However, Pure SA/CS hydrogels still have room for improvement in adsorption performance, mechanical strength, thermal stability, and swelling behavior. Forming composites with carbon-based materials is a common and effective optimization strategy [23]. Typical carbon-based materials such as biochar [24], graphene [25] and carbon nanotubes [26] have been widely used in hydrogel modification due to their excellent structure and properties. As fabricated by He [27] et al., the SA-KBC-Fe/La composite hydrogel possesses a maximum phosphate adsorption capacity that is threefold higher than that of the biochar-free counterpart. Among them, activated carbon (AC) as a typical carbonaceous material, not only possesses a high specific surface area, well-developed hierarchical pores and abundant surface oxygen-containing functional groups [28], but also can directly interfere with the physiological activities of algal cells and exert an algal inhibition effect through its surface chemical properties (e.g., persistent free radicals, C and O content) [29]. These studies indicate that the introduction of AC can effectively improve the material properties, algal inhibition effect, and allelochemical encapsulation efficiency of SA/CS gel microspheres. However, systematic studies on the formulation optimization, algal inhibition performance, and sustained-release behavior of SA/CS/AC gel microspheres loaded with citrus peel extract are still lacking.

To improve the stability and long-term algal inhibition efficiency of natural allelochemicals and achieve the resource utilization of citrus peel agricultural waste, this study used citrus peel extract as the algal inhibitory functional component and anhydrous calcium chloride as the cross-linking agent to fabricate SA/CS/AC gel microspheres sustained-release materials. By optimizing the mass ratio of SA, CS, and AC, the characterization, sustained-release properties, and algal inhibition performance of the gel microspheres were investigated, and the optimal preparation ratio was further determined. This work aims to provide new ideas and a scientific basis for the application of such gel microspheres in the field of algal inhibition.

 doi:10.20944/preprints202604.2211.v1

2. Results and Discussion

2.1. Optimization and Interpretation Based on Response Surface Methodology

2.1.1. Experimental Data Basis for Response Surface Optimization

A three-factor, three-level response surface methodology (Box–Behnken design) was employed with algal inhibition rate as the response value. The independent variables were SA concentration (A), CS concentration (B), and AC concentration (C) (Table 1). The algal inhibition rates of the 17 runs ranged from 66.74% to 86.55%. All repeated central point experiments exhibited inhibition rates above 83%, indicating good experimental stability. A regression model was constructed via Design-Expert to link dosing concentrations to algal inhibition rate (Y).

$$Y = 85.21 - 0.52 * A + 0.64 * B + 1.61 * C + 1.35 * AB + 1.77 * AC - 3.51 * BC - 2.55 * A^2 - 3.48 * B^2 - 9.68 * C^2 \quad (1)$$

In this equation, Y represents the algal inhibition efficiency of the gel microspheres material. (w/v, %). A is the sodium alginate concentration (w/v, %). B is the chitosan concentration (w/v, %). and C is the activated carbon concentration (w/v, %).

Table 1. Design matrix and measured responses for the response surface optimization.

Serial Number	A (%)	B (%)	C (%)	Inhibition rate (%)
1	2	0.4	0.2	66.74
2	2	1.3	0.2	73.95
3	2.5	0.4	0.3	75.21
4	2	0.7	0.3	84.10
5	2.5	0.7	0.4	76.62
6	2.5	0.7	0.2	70.08
7	2	0.7	0.3	85.12
8	2.5	1.3	0.3	80.29
9	2	1.3	0.4	70.35
10	1.5	0.7	0.2	72.86
11	1.5	1.3	0.3	80.43
12	2	0.7	0.3	83.89
13	2	0.7	0.3	86.37
14	1.5	0.7	0.4	72.34
15	2	0.7	0.3	86.55
16	1.5	0.4	0.3	80.76
17	2	0.4	0.4	77.16

Note: A, B, and C correspond to the concentrations of SA, CS, and AC (%), in that order.

2.1.2. Regression Model Development and ANOVA Significance Analysis

The Analysis of variance (ANOVA) results (Table 2) confirmed that the regression model exhibited extremely high significance ($F = 31.16$, $p < 0.0001$), with a non-significant lack-of-fit term ($p = 0.2650$). The determination coefficient $R^2 = 0.9756$, adjusted $R^2 = 0.9443$, Both values were close to 1, indicating high reliability of the model [30]. coefficient of variation = 1.18% (< 10%), and adequate precision = 16.8254 (> 4), indicating high goodness of fit and reliability for predicting the relationship between preparation parameters and algal inhibition rate.The significant influencing factors ($p < 0.05$) were C, AC, BC, A^2, B^2, and C^2. The order of influence on algal inhibition rate was: AC content (C) >

 doi:10.20944/preprints202604.2211.v1

CS content (B) > SA content (A). The quadratic regression model was effective for investigating and identifying the optimum formulation parameters of the SA/CS/AC gel microspheres.

Table 2. ANOVA for the quadratic regression model.

Source	Sum of Squares	d/f	Mean Square	F-Value	*p*-Value	
Model	602.18	9	66.91	31.16	＜0.0001	Significant
A	2.19	1	2.19	1.02	0.3457	
B	3.32	1	3.32	1.54	0.2540	
C	20.61	1	20.61	9.60	0.0174	
AB	7.32	1	7.32	3.41	0.1074	
AC	12.46	1	12.46	5.80	0.0468	
BC	49.14	1	49.14	22.88	0.0020	
A^2	27.47	1	27.47	12.79	0.0090	
B^2	50.97	1	50.97	23.74	0.0018	
C^2	394.27	1	394.27	183.61	＜0.0001	
Residual	15.03	7	2.15			
Lack of Fit	8.91	3	2.97	1.94	0.2650	Not significant
Pure Error	6.12	4	1.53			
Cor Total	617.22	16				
			R^2=0.9756; Adjusted R^2=0.9443			
			CV=1.88%; Adeq Precision=16.8254			

Note: A, B, and C correspond to the concentrations of SA, CS, and AC (%), in that order.

2.1.3. Analysis of Response Surface Interactions

2D contour and 3D response surface plots were generated using Design-Expert to evaluate the effects of sodium alginate (A), chitosan (B), and activated carbon (C) concentrations on the algal inhibition rate of SA/CS/AC gel microspheres. Based on the quadratic regression model, interaction effects were analyzed. The slope and curvature of the response surfaces reflect factor effects and interactions, while contour density indicates their relative significance [31].

As shown in Figure 1, the effects and interactions of sodium alginate (A), chitosan (B), and activated carbon (C) on the algal inhibition rate of the gel microspheres were systematically analyzed by fixing each single factor at the central point level.

When C was fixed at 0.3% (Figure 1(a)), the response surface showed a gentle slope, and the contour plot was approximately circular with sparse distribution, which was consistent with ANOVA. These results indicated that both the main effects of A and B and their interaction were weak. Nevertheless, the algal inhibition rate first increased and then decreased with increasing A and B concentrations, showing a quadratic response dominated by their significant quadratic terms.Insufficient concentrations led to poor microsphere formation and insufficient active component loading, while excessive concentrations resulted in a dense gel network that hindered the release of active substances, both of which reduced algal inhibition efficiency.

 doi:10.20944/preprints202604.2211.v1

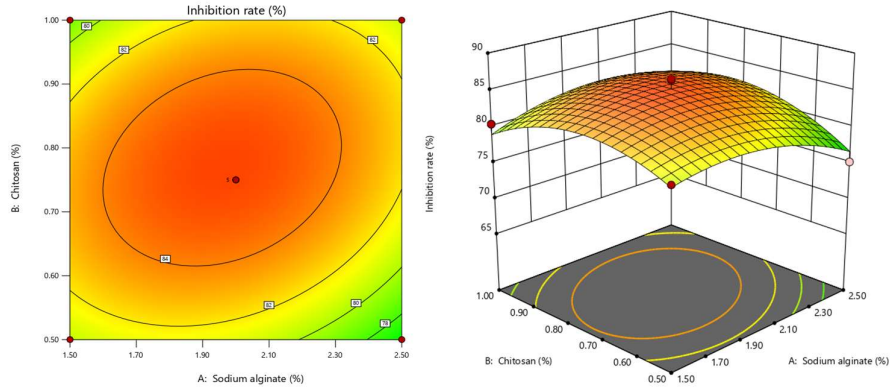

(a) Interaction between A and B

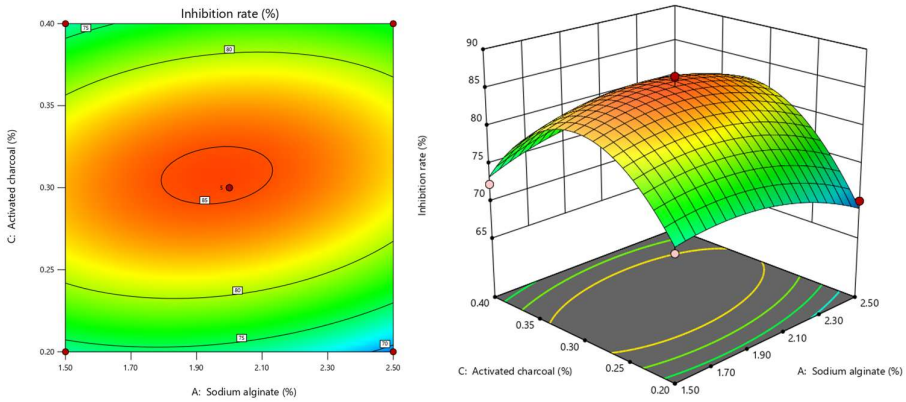

(b) Interaction between A and C

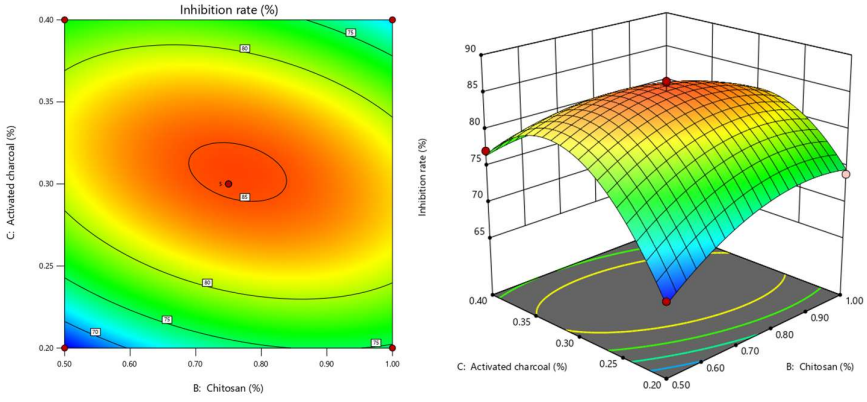

(c) Interaction between B and C

Figure 1. Response surface and contour plots showing the interactive effects of sodium alginate (A), chitosan (B), and activated carbon (C) concentrations on the algal inhibition rate of SA/CS/AC gel microspheres. (a): Interaction between A and B; (b): Interaction between A and C; (c): Interaction between B and C.

When B was fixed at 0.75% (Figure 1(b)), the response surface was steeper along the C axis, and the contour lines were typically elliptical and densely distributed along C, visually indicating that the main effect of C was significantly stronger than that of A, with a significant interaction between them. The influence order was C > A. The algal inhibition rate exhibited a quadratic change with increasing A and C concentrations. This nonlinear response was jointly dominated by their significant

 doi:10.20944/preprints202604.2211.v1

quadratic and interactive terms. Deviation from the optimal concentration range caused insufficient active component loading, activated carbon aggregation, or structural damage to the gel matrix, thereby significantly reducing the algal inhibition effect. The algal inhibition rate showed a quadratic variation with increasing A and C concentrations. This nonlinear response was governed by their significant quadratic and interactive terms. Deviation from the appropriate concentration range resulted in insufficient loading of active components, activated carbon aggregation, or structural destruction of the gel matrix, thus markedly weakening the algal inhibition performance.

When A was fixed at 2.5% (Figure 1(c)), the response surface was steep along B and C axes with a distinct peak, and the contour lines exhibited an elliptical shape with an inclined major axis, confirming a strong synergistic interaction between B and C. The contour lines were more densely distributed along the C axis, indicating that the effect of C was significantly stronger than that of B. The extreme concentration regions corresponded to the optimal balance between adsorption capacity and sustained-release performance.

Overall, the order of influencing factors on algal inhibition rate was: activated carbon content > chitosan content > sodium alginate content.

2.1.4. Optimization of Preparation Parameters and Model Validation

As shown in Figure 2, the optimal preparation parameters of the SA/CS/AC gel microspheres were optimized by Design-Expert software: 1.97% SA, 0.76% CS, and 0.31% AC (within the factor level range), with a predicted algal inhibition rate of 85.29%.The experimental algal inhibition rate from three parallel validation tests was 85.17±2.49%, which agreed well with the predicted value, verifying the reliability of the model.

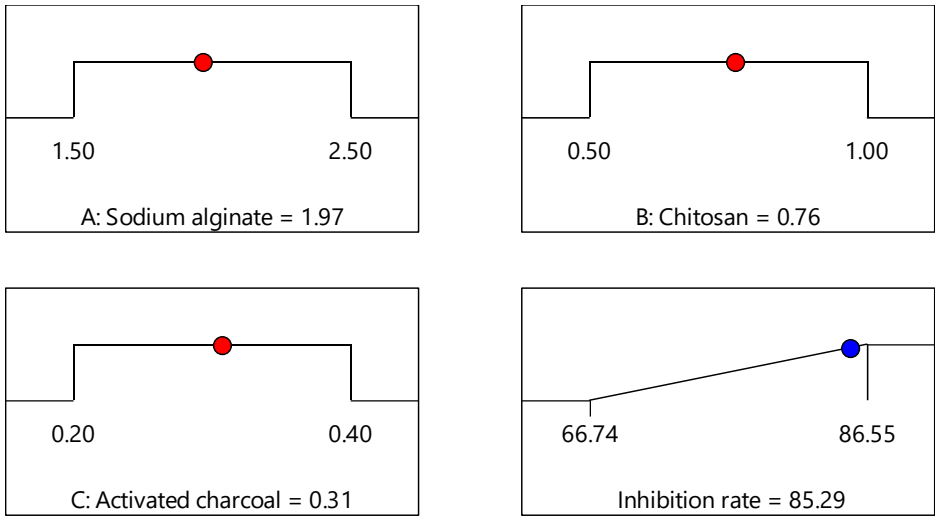

Figure 2. Optimal formulation concentrations and responses via response surface optimization.

2.2. Release Curve of the SA/CS/AC Gel Microspheres Material

The release performance of the composite gel material is a core indicator for evaluating its environmental application potential, which directly determines the utilization efficiency and ecological safety of allelochemicals. The standard curve for total phenolics in citrus peel was $y = 0.0514x + 0.0165$ ($R^2 = 0.9723$), which exhibited a good linear relationship within the experimental concentration range, indicating that ultraviolet spectrophotometry is effective for determining allelochemical content in citrus peel. Cumulative release of citrus peel allelochemicals from the SA/CS/AC microspheres was measured over 25 days (Figure 3), and the release curve is shown below.

 doi:10.20944/preprints202604.2211.v1

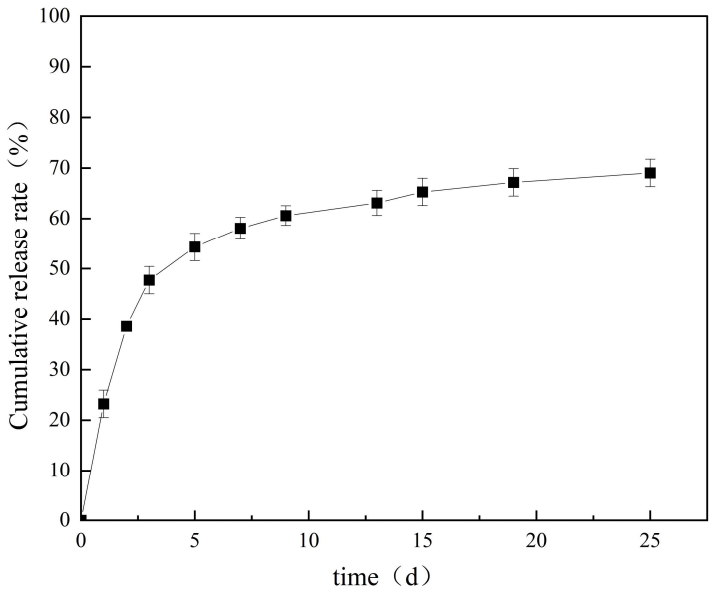

Figure 3. Cumulative release curve of the SA/CS/AC composite gel material.

The allelochemical release from the gel microspheres exhibited a biphasic characteristic of "rapid release - sustained release" : the first 0–5 days corresponded to the rapid release phase, where the surface-adsorbed allelochemicals were rapidly desorbed, achieving a cumulative release rate of 55% to quickly inhibit algal proliferation; the period from 5 to 25 days was the sustained release phase, during which the allelochemicals slowly diffused through the porous structure of the gel microspheres, with the cumulative release rate reaching 70%, realizing long-term algal inhibition. As the diffusion path of allelochemicals within the SA/CS/AC gel microspheres lengthened and the mass transfer resistance of the polymer matrix increased over time, the release rate gradually decelerated and eventually plateaued, reaching a cumulative release of approximately 70% by day 25.

This release profile demonstrates the excellent sustained-release properties of the gel microspheres. It not only achieves immediate algal inhibition via the initial rapid release but also maintains an effective concentration of allelochemicals in the water through the subsequent stable release. This prolongs the duration of efficacy and avoids the drastic concentration fluctuations typically associated with direct application.

2.3. Materials Characterization

2.3.1. SEM Characterization of the SA/CS/AC Gel Microspheres

As observed in Figures 4(a) and (b), the SA/CS/AC composite exhibits an irregular ellipsoid-like morphology with evident surface collapse, wrinkling, and local lamellar delamination, which can be attributed to structural shrinkage and reconstruction induced by water migration during freeze-drying [32]. At higher magnifications (Figures 4(c) and (d)), distinct interlayer gaps are observed. The combined structure of wrinkles, lamellae, and gaps is conducive to increasing interfacial contact area and may facilitate adsorbate diffusio [33]. The current observations corroborate the conclusions reported in the study by Huang and colleagues [34].

 doi:10.20944/preprints202604.2211.v1

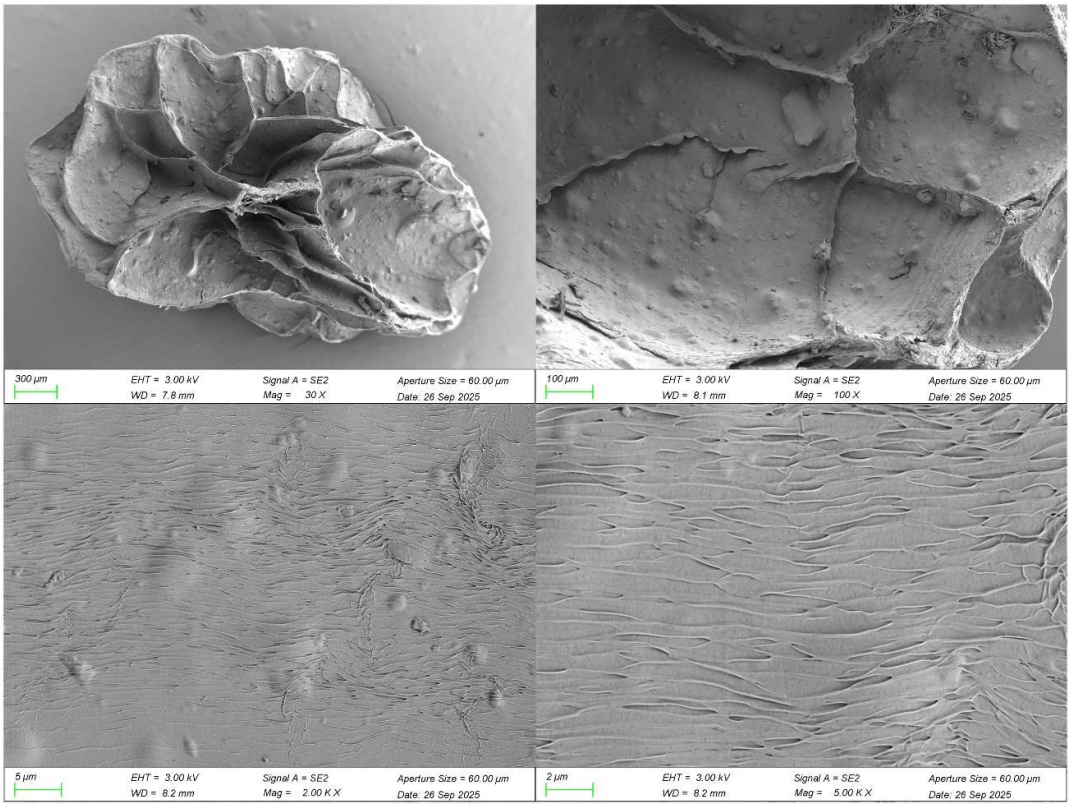

Figure 4. Scanning electron microscopy of SA/CS/AC composite gel material surface.

2.3.2. Functional Groups of SA/CS/AC Gel Microspheres

As illustrated in Figure 5, broad absorption bands are observed at 3345 cm^{-1} and 3317 cm^{-1} in the spectra of both SA/CS gel microspheres and SA/CS/AC gel microspheres. These peaks come from –OH and –NH stretching vibrations, indicating hydrogen-bonding networks in the gel microspheres matrix [35]. Compared to SA/CS, this band shifts slightly to a lower wavenumber (3317 cm^{-1}) in SA/CS/AC, which points to stronger hydrogen bonding after adding activated carbon. Distinct absorption features at ~1593 cm^{-1} and 1413 cm^{-1} arise from the asymmetric and symmetric stretching vibrations of carboxyl groups (COO^-), respectively. The 1027 cm^{-1} and 1021 cm^{-1} bands are attributed to C–O stretching and C–O–C linkages in the polysaccharide backbone [36]. These characteristic peaks are retained in the composite, indicating that the fundamental structure of SA/CS remains intact. A new peak at 2930 cm^{-1}, assigned to C–H stretching, appears in SA/CS/AC. The intensities of the 1592 cm^{-1}, 1414 cm^{-1}, and 1021 cm^{-1} bands also increase, likely due to activated carbon and its surface oxygen-containing groups [37]. These results indicate that adding activated carbon changes the surface chemical environment to enhance the loading and sustained release of citrus peel allelochemicals.

 doi:10.20944/preprints202604.2211.v1

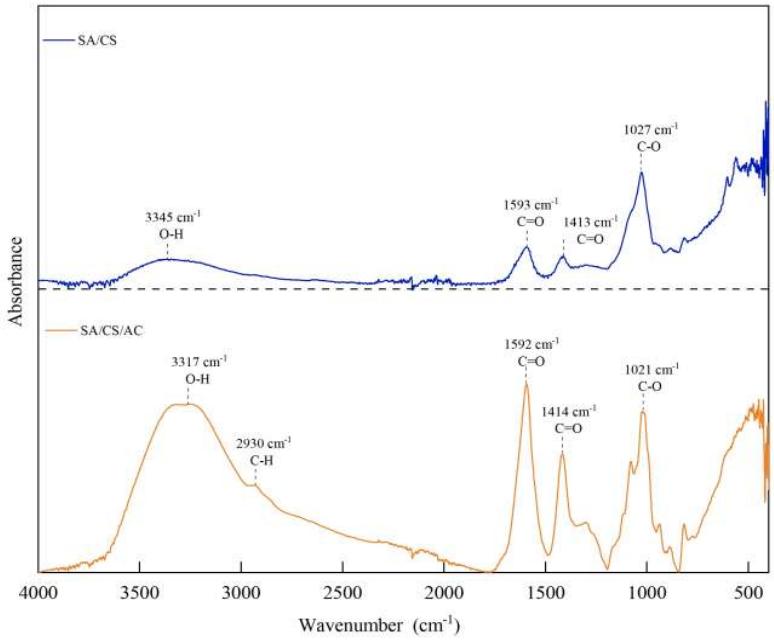

Figure 5. Infrared spectra of SA/CS gel microspheres and SA/CS/AC gel microspheres.

2.3.3. LC-MS Identification of Core Allelochemicals in Citrus Peel Extract

Qualitative analysis was performed using ultra-high-performance liquid chromatography-quadrupole time-of-flight tandem mass spectrometry (UHPLC-QTOF-MS/ MS). The system was operated in negative electrospray ionization（ESI^-） mode. Chemical structures were confirmed by MS/MS fragmentation pattern analysis and database matching (matching score ⩾80, mass-to-charge ratio deviation < 1 ppm), with detailed chromatographic conditions provided in Section 4.2.2.

As shown in Table 3, 20 common allelopathically active compounds were detected, with 19 phenolic substances (dominant components) including phenolic acids (e.g., benzoic acid, cinnamic acid) and flavonoids.

Table 3. LC-MS Qualitative Identification Results of Common Allelochemicals.

Serial Number	Retention Time	Molecular Formula	M/Z	Mass Deviation /ppm	Compound Name	Category	Matching Score
1	0.645	$C_7H_{12}O_6$	191.0560	−0.33	D-(-)-Quinic acid	Organic acid	99.86
2	0.732	$C_4H_6O_5$	133.0142	−0.56	Malic acid	Organic acid	99.9
3	0.849	$C_9H_{13}NO_2$	166.0875	0.72	Synephrine	Alkaloid	99.35
4	1.584	$C_7H_6O_4$	153.0194	0.47	Protocatechuic acid	Phenolic acid	99.24
5	1.994	$C_7H_6O_3$	137.0243	−0.59	p-hydroxybenzoic acid	Phenolic acid	99.76
6	2.244	$C_7H_6O_2$	121.0295	−0.17	Benzoic Acid	Phenolic acid	99.98
7	2.288	$C_8H_8O_4$	167.0350	0.14	Vanillic acid	Phenolic acid	98.87
8	2.731	$C_8H_8O_5$	183.0298	−0.30	Methyl gallate	Phenolic acid	97.08
9	3.823	$C_9H_8O_3$	163.0400	−0.26	p-Coumaric acid	Phenolic acid	98.01
10	1.332	$C_7H_{10}O_5$	173.0455	−0.22	Shikimic acid	Organic acid	98.22
11	4.927	$C_{27}H_{32}O_{15}$	595.1666	−0.48	Neoeriocitrin	Flavonoid	98.74
12	5.370	$C_{27}H_{32}O_{14}$	579.1717	−0.45	Naringin	Flavonoid	99.41
13	5.813	$C_{28}H_{34}O_{15}$	609.1821	−0.68	Neohesperidin	Flavonoid	99.16

 doi:10.20944/preprints202604.2211.v1

14	5.916	$C_{21}H_{20}O_{11}$	447.0929	−0.89	Quercetin 7-rhamnoside	Flavonoid	97.69
15	6.494	$C_{16}H_{14}O_6$	301.0716	−0.47	Hesperetin	Flavonoid	83.96
16	6.539	$C_{21}H_{20}O_{12}$	463.0879	−0.68	Isoquercitrin	Flavonoid	95.64
17	6.509	$C_{27}H_{30}O_{16}$	609.1461	−0.02	Kaempferol 3-O-sophoroside	Flavonoid	99.73
18	2.746	$C_{10}H_8O_3$	175.0401	0.07	7-Methoxycoumarin	Coumarins	98.18
19	10.067	$C_{14}H_{28}O_2$	227.2018	0.43	Myristic acid	Fatty acid	99.77
20	10.471	$C_{18}H_{32}O_2$	279.2328	−0.63	Linoleic acid	Fatty acid	97.83

Based on the LC-QTOF-MS/MS analysis, three groups of components were separated according to polarity.The strongly polar components were eluted within 0.5-4 min, mainly including organic acids and small phenolic acids.Medium-polar components were eluted at 4-7 min, which were dominated by flavone glycosides, with hesperetin as the most abundant constituent.Weakly polar components were eluted at 7-16 min, mainly composed of flavone aglycones and fatty acids.

Due to their stronger polarity, phenolic acids generally exhibit shorter retention times than flavonoids on reversed-phase C18 columns. Their tandem mass spectrometry fragmentation is dominated by the loss of neutral small molecules, and the fragmentation patterns are closely related to their skeleton types, as well as the types and numbers of substituents [38]. For phenolic acids devoid of methoxyl substituents (e.g., protocatechuic acid [39], p-coumaric acid, 4-hydroxybenzoic acid [40]), the dominant fragmentation mechanism proceeds through C–O bond scission in the carboxyl moiety, leading to the elimination of CO_2 (44 Da). Subsequent secondary fragmentations encompass the dehydration of phenolic hydroxyl groups (H_2O, 18 Da) and cyclization-induced CO loss (28 Da). The fragmentation behavior of methoxyl-substituted phenolic acids varies with substitution patterns: monomethoxylated derivatives (e.g., vanillic acid, ferulic acid) preferentially eliminate a methyl radical ($\bullet CH_3$) under ESI^- mode, followed by CO_2 loss; dimethoxylated derivatives (e.g., syringic acid, sinapic acid) follow a similar pathway, with further subsequent loss of methoxy radical ($–OCH_3$) or formaldehyde (CH_2O) [41].

Neoeriocitrin and kaempferol 3-O-sophoroside produced stable deprotonated molecular ions $[M–H]^-$ at m/z 595.1677 and 609.1813, respectively, in ESI^- mode. Upon collision-induced dissociation, both underwent preferential glycosidic bond cleavage, losing a rhamnosyl-glucosyl moiety (308.1107 Da) and a sophorosyl moiety (308.0743 Da), respectively, yielding distinct aglycone-derived diagnostic fragment ions at m/z 287.0561 and 301.0712. Further secondary fragmentation occurred with the loss of neutral small molecules, including CO (27.9949 Da) for neoeriocitrin and CO (27.9949 Da) plus C_3O_2 (68.0002 Da) for kaempferol 3-O-sophoroside, producing fragments such as m/z 567.1709 and m/z 286.0481. These fragmentation behaviors are consistent with the typical pattern of flavonoid glycosides, characterized by preferential glycosidic bond cleavage followed by sequential neutral loss from the aglycone [42]. The other five flavonoid compounds, namely naringin, neohesperidin, quercetin 7-rhamnoside, hesperetin, and isoquercitrin, were tentatively identified based on accurate mass measurements (mass deviation < 5 ppm), molecular formula matching, and database searching. Their elution order followed the structure-retention relationship of flavonoids, with more polar glycosides eluting first and less polar aglycones eluting later [43], supporting the reliability of the tentative identification. Flavonoid glycosides exhibited obvious gradient elution characteristics due to the difference in glycosyl substituents (Table 3). Neoeriocitrin (disaccharide substitution, 4.927 min) and naringin (disaccharide substitution, 5.370 min) were eluted earlier than quercetin 7-rhamnoside (monosaccharide substitution, 5.916 min), indicating that the increase in glycosyl number leads to stronger polarity and shorter retention time on reversed-phase C18 column.

2.4. Algae Inhibition Experiments of SA/CS/AC Gel Microspheres

Chlorophyll-a (Chl-a) concentration acts as a pivotal metric for algal photosynthetic activity, enabling indirect assessment of algal physiological state and viability [44]. Changes in Chl-a content

 doi:10.20944/preprints202604.2211.v1

of *Microcystis aeruginosa* under different treatments are shown in Figure 6. The results indicate that, compared with the blank control, SA/CS/AC gel microspheres at all tested concentrations (3-5 g/L) significantly inhibited Chl-a accumulation ($P < 0.05$), and the inhibitory effect increased with increasing material concentration. Algal inhibition decreased slightly from day 7 to 30, owing to sustained allelochemical consumption and limited loading, which lowered the effective concentration. Nevertheless, the 5 g/L group still maintained a 76.27% inhibition rate on day 30, with chlorophyll-a content of only 2.48 mg/L (23.67% of the control).However,the maximum inhibition rate of the carbon-free control group (SA/CS gel microspheres) was only about 52.81%. The blank SA/CS/AC carrier (without loading citrus peel allelochemicals) reduced the chlorophyll concentration of *Microcystis aeruginosa* by 30.58%, confirming the intrinsic algal inhibition activity of AC. Abundant persistent free radicals and oxygen-containing surface functionalities (e.g., –OH and C=O) on the AC surface may disrupt the photosynthetic system of *Microcystis aeruginosa*, resulting in reduced chlorophyll a synthesis efficiency, in agreement with previous studies [45,46]. After loading allelochemicals, the algal inhibition rate of the SA/CS/AC gel microspheres further increased to 76.27%, indicating that the intrinsic inhibition of AC and the chemical inhibition of citrus peel allelochemicals generated a physico–chemical synergistic effect that significantly enhanced the algal inhibition performance.

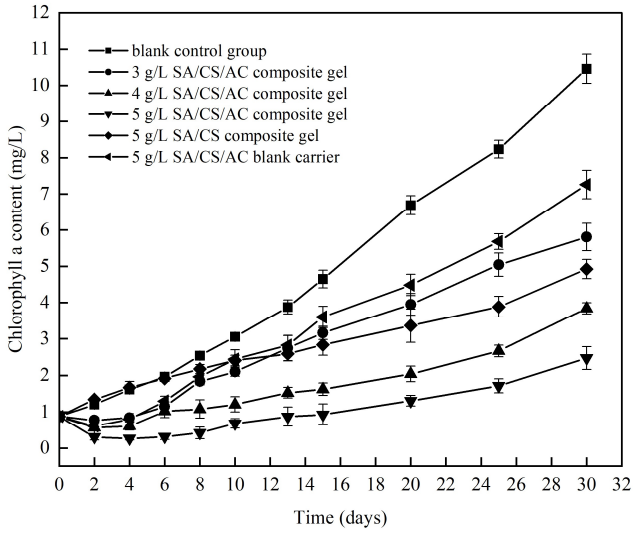

Figure 6. Effects of blank SA/CS/AC carrier, SA/CS gel microspheres, and SA/CS/AC gel microspheres on the chlorophyll-a content in *Microcystis aeruginosa* cells. Note: Blank SA/CS/AC carrier refers to the gel microspheres without loading citrus peel allelochemicals. SA/CS and SA/CS/AC gels are loaded with allelochemicals from citrus peel.

3. Conclusions

In this study, we successfully prepared a SA/CS/AC gel microspheres loaded with allelochemicals from citrus peel, and applied it to inhibit *Microcystis aeruginosa*. Preparation parameters were optimized using Box–Behnken design and response surface methodology. The optimal mass fractions of SA, CS, and AC were determined to be 1.97%, 0.76%, and 0.31%, respectively. Experimental validation confirmed that the regression model was reliable and exhibited satisfactory predictive power.The gel microspheres exhibited a typical rapid initial release followed by slow release. The gel microspheres released allelochemicals quickly in 0–5 days and steadily up to 25 days. Around 70% was released over 25 days. SEM and FT-IR analyses showed that the gel microspheres had a well-developed porous structure and abundant surface functional groups, enabling it to effectively load allelochemicals from citrus peel. Due to the continuous consumption of allelochemicals and limited loading capacity, the algal inhibition rate decreased slightly from day 7

 doi:10.20944/preprints202604.2211.v1

to day 30. However, at a dosage of 5 g/L, the inhibition rate still remained above 76% after 30 days. The algal inhibition rates of blank SA/CS/AC carrier (without allelochemicals) and the AC-free SA/CS gel microspheres were only 30.58% and 52.81%, respectively. This shows that incorporating activated carbon into the carrier together with citrus peel allelochemicals can significantly improve algal inhibition efficiency. This study provides a feasible and eco-friendly technical approach for the sustainable control of cyanobacterial blooms.

4. Materials and Methods

4.1. Materials

Fresh citrus peels were obtained from a local market located near the university campus. The *Microcystis aeruginosa* FACHB-912 isolate employed in the present study was sourced from the Freshwater Algae Culture Collection, Institute of Hydrobiology, Chinese Academy of Sciences. BG11 medium for algal cultivation was purchased from Qingdao Haibo Biotechnology Co., Ltd. (China). Sodium alginate (analytical grade) was provided by Sinopharm Chemical Reagent Co., Ltd. Supplementary reagents, including anhydrous calcium chloride, chitosan, activated carbon, acetone, hydrochloric acid, methanol, and glacial acetic acid, were all of analytical quality and procured from Chengdu Kelong Chemical Co., Ltd. (China).

4.2. Material Synthesis and Optimization

4.2.1. Preparation of Citrus Peel Extract

Citrus peel (Citrus reticulata) was freeze-dried for 24 h, ground, and sieved (100 mesh). Powder extraction was performed with 80% methanol (1:20, w/v) at 70 °C over a 2-hour period. Post-extraction, the suspension was left to cool naturally and then clarified through filtration. The filtrate was stored at 4 °C prior to further analysis.

4.2.2. LC–MS Characterization of Citrus Peel Extracts

Before the formal chromatographic detection process, all samples were treated by filtration through a 0.22 μm membrane filter, aiming to eliminate particulate impurities present in the samples. Chromatographic separation was carried out on a reversed-phase C18 column using a binary mobile phase system consisting of 0.1% formic acid in water (phase A) and methanol (phase B), delivered at 0.3 mL/min. The elution was conducted under a programmed gradient as follows: initially 95% A (0-1.5 min), decreased to 60% A (1.5-5 min), further reduced to 5% A (5-17 min), and finally returned to initial conditions for column equilibration.

4.2.3. Synthesis of SA/CS/AC Gel Microspheres

The preparation strategy was adapted from a previously reported method by Bustos et al., with modifications to suit the current experimental design [47]. Sodium alginate was solubilized in deionized water, then combined with citrus peel extract and activated carbon to yield a homogeneous precursor solution. The resulting mixture was then gradually introduced into a crosslinking solution containing chitosan and $CaCl_2$, with the pH adjusted to 4.5, under continuous stirring. Following the crosslinking reaction, the microspheres specimens were thoroughly washed with ultrapure water to remove remnant unreacted species, and then lyophilized for subsequent experimental use.

4.2.4. RSM-Based Experimental Optimization via Response Surface Methodology

Optimization of gel microspheres formulation was conducted using a three-factor, three-level Box–Behnken experimental design. The concentrations of sodium alginate (A), chitosan (B), and activated carbon (C) were chosen as the independent experimental factors, with the algal inhibition rate (Y) set as the response variable (Table 4).

 doi:10.20944/preprints202604.2211.v1

Table 4. Experimental variables and coded levels for the Box–Behnken response surface design.

Factor	Code	The Level of Code		
		-1	0	1
Sodium alginate concentration (w/v, %)	A	1.5	2	2.5
Chitosan concentration (w/v, %)	B	0.4	0.7	1
activated carbon concentration (w/v, %)	C	0.2	0.3	0.4

4.3. Assessment of Total Phenolics in Citrus Peel Extract

The total phenolic content in both citrus peel extract and gel microspheres samples was quantified using the Folin–Ciocalteu assay [48]. Gallic acid was selected as the reference standard to construct a calibration model, which exhibited a strong linear correlation within the tested concentration range ($y = 0.0187x + 0.0101, R^2 = 0.9748$). This relationship enabled reliable estimation of phenolic content and provided a quantitative basis for evaluating the loading of bioactive compounds.

4.4. Material Characterization

The surface morphology and microstructure of the SA/CS/AC gel microspheres were characterized by SEM (ZEISS Sigma 360). Samples were dried, mounted on conductive adhesive tape, and cleaned with a rubber bulb prior to observation. Images were acquired at magnifications ranging from 30 to 50,000×.

Fourier transform infrared spectroscopy (FTIR) was employed to analyze the chemical structure of the gel microspheres. Dried samples were ground with spectroscopic-grade KBr, pressed into pellets, and analyzed over the range of 4000–500 cm^{-1}.

4.5. Algal Growth Inhibition Experiment

4.5.1. Cultivation of *Microcystis aeruginosa*

Algal cultures were maintained in BG11 medium under controlled laboratory conditions. Cells were grown to the exponential phase at 25±0.5°C, with a light intensity of 1500-2200 lx and a 12 h light/dark photoperiod to ensure stable growth dynamics.

4.5.2. Algal Growth Inhibition Experiment of SA/CS/AC Gel Microspheres

Gel microspheres samples were applied to 150 mL algal cultures at final concentrations of 3.0, 4.0, and 5.0 g/L. A control without gel microspheres was included. All treatments were performed in triplicate over 30 days, and Chl-a content was periodically measured to assess algal inhibition performance.

4.5.3. Algal Growth Inhibition Rate

The inhibition rate of *Microcystis aeruginosa* growth by the SA/CS/AC gel microspheres was evaluated based on Chl-a content [49], calculated as:

$$IR=(1-N_t/N_0)\times 100\% \quad (2)$$

where IR represents the inhibition rate, and Nt and N_0 represent the chl-a contents (mg/L) in the treatment and blank control groups, respectively.

Chlorophyll-a content was quantified using an acetone extraction procedure combined with spectrophotometric analysis [50]. Absorbance values were recorded at 630, 645, 663, and 750 nm, and the concentration was calculated according to the following equations.

 doi:10.20944/preprints202604.2211.v1

$$C=11.64(A_{663}-A_{750})-2.16(A_{645}-A_{750})+0.1(A_{630}-A_{750}) \quad (3)$$

$$\text{Chl-a}=\frac{CV_1}{V_2} \quad (4)$$

A_{630}, A_{645}, A_{663}, and A_{750} are the absorbance values at 630, 645, 663, and 750 nm, respectively. V_1 and V_2 denote the volumes (mL) of algal suspension and 90% acetone, respectively. The calculated Chl-a parameter corresponds to the chl-a content, reported in mg/L.

4.6. Data Analysis

All analytical measurements were repeated in three independent replicates, and the resultant data are expressed as mean values. Data processing was carried out using Microsoft Excel 2021, while graphical visualization was completed with Origin 2021. Response surface modeling and statistical analysis were conducted using Design-Expert 13.

Author Contributions: Y.W. and D.J. designed the research framework. D.J. conducted the experiments and performed data analysis. Y.W. provided supervision and contributed to methodological development. The manuscript was initially drafted by D.J., and both authors participated in revising and improving the final version. All contributing authors have verified the accuracy of the published manuscript and signed off on its final form for publication.

Funding: This research did not receive any financial support from external sources.

Institutional Review Board Statement: Not applicable.

Informed Consent Statement: Not applicable.

Data Availability Statement: All raw data supporting the findings of this work are accessible from the lead contact author upon request.

Conflicts of Interest: No potential conflict of interest was reported by the authors.

References

1. Yancey, C.E.; Smith, D.J.; Den Uyl, P.A.; Mohamed, O.G.; Yu, F.; Ruberg, S.A.; Chaffin, J.D.; Goodwin, K.D.; Tripathi, A.; Sherman, D.H.; Dick, G.J. Metagenomic and Metatranscriptomic Insights into Population Diversity of Microcystis Blooms: Spatial and Temporal Dynamics of mcy Genotypes, Including a Partial Operon That Can Be Abundant and Expressed. *Appl. Environ. Microbiol.* **2022**, 88, e02464-21.
2. Qin, B.Q.; Deng, J.M.; Shi, K.; Wang, J.; Brookes, J.; Zhou, J.; Zhang, Y.L.; Zhu, G.W.; Paerl, H.W.; Wu, L. Extreme climate anomalies enhancing cyanobacterial blooms in eutrophic Lake Taihu, China. *Water Resour. Res*. **2021**, 57, e2020WR029371.
3. Xu, S.S.; Yi, X.P.; Liu, W.Y.; Zhang, C.C.; Massey, I.Y.; Yang, F.; Tian, L. A review of nephrotoxicity of microcystins. *Toxins* **2020**, 12, 693.
4. Zeng, G.M.; Zhang, R.; Liang, D.; Wang, F.; Han, Y.G.; Luo, Y.; Gao, P.; Wang, Q.F.; Wang, Q.H.; Yu, C.Y.; Jin, L.B.; Sun, D., Comparison of the advantages and disadvantages of algae removal technology and its development status. *Water* **2023**. 15, 1104.
5. Zhu, X.Q.; Dao, G.H.; Tao, Y.; Zhan, X.M.; Hu, H.Y. A review on control of harmful algal blooms by plant-derived allelochemicals. *J. Hazard. Mater.* **2021**, 401, 123403.
6. Li, B.H.; Yin, Y.J.; Kang, L.F.; Feng, L.; Liu, Y.Z.; Du, Z.W.; Tian, Y.J.; Zhang, L.Q. A review: application of allelochemicals in water ecological restoration——algal inhibition. *Chemosphere* **2021**, 267, 128869.
7. Wang, T.T.; Liu, H.C. Aquatic plant allelochemicals inhibit the growth of microalgae and cyanobacteria in aquatic environments. *Environ. Sci. Pollut. Res.* **2023**, 30, 105084-105098.
8. Cao, J.G.; Dong, Z.Z.; Zhao, H.Y.; Duan, S.H.; Cao, X.L.; Liu, H.L.; Yang, Z.Z. Allelopathic effect of rhubarb extracts on the growth of *Microcystis aeruginosa*. *Water Sci. Technol.* **2020**, 82, 1092-1101.

 doi:10.20944/preprints202604.2211.v1

9. Soares, C.; Moreira, M.M.; Ramos, S.; Ramalhosa, M.J.; Correia, M.; Svarc-Gajić, J.; Delerue-Matos, C.; Barroso, M.F. A critical assessment of extraction methodologies for the valorization of agricultural wastes: Polyphenolic profile and bioactivity. *Processes* **2023**, 11, 1767.
10. Chatzimitakos, T.; Athanasiadis, V.; Kotsou, K.; Bozinou, E.; Lalas, S.I. Response surface optimization for the enhancement of the extraction of bioactive compounds from Citrus limon peel. *Antioxidants* **2023**, 12, 1605.
11. Amoriello, T.; Mellara, F.; Ciorba, R.; Ceccarelli, D.; Amoriello, M.; Taddei, F.; Ciccoritti, R. Phenols Extraction from Sorghum Byproducts: Upcycling Strategies and Food Applications. *Antioxidants* **2025**, 14, 668.
12. Kaur, S.; Ubeyitogullari, A. Extraction of phenolic compounds from rice husk via ethanol-water-modified supercritical carbon dioxide. *Heliyon* **2023**, 9, e14196.
13. Srisaikham, S. A comparison of nutritional values, bioactive compounds, amino acids, and antioxidant activities of alfalfa (Medicago sativa) plant and Pellet for use as beneficial material ruminant feed. *Walailak J. Sci. Technol.* **2021**, 18, 10312-16.
14. Zhang, X.; Hu, H.Y. Inhibitory Effect of Aqueous Citrus Peel Extract on the Growth of *Microcystis aeruginosa*. *Res. Environ. Sci.* **2008**, 21, 43-48.
15. Mushtaq, W.; Fauconnier, M.-L. Phenolic profiling unravelling allelopathic encounters in agroecology. *Plant Stress* **2024**, 13, 100523.
16. Cheng, K.; Zhao, K.; Zhang, R.; Guo, J.F. Progress on control of harmful algae by sustained-release technology of allelochemical: A review. *Sci. Total Environ.* **2024**, 918, 170364.
17. Garcia-Garcia, A.; Muñana-González, S.; Lanceros-Mendez, S.; Ruiz-Rubio, L.; Alvarez, L.P.; Vilas-Vilela, J.L. Biodegradable natural hydrogels for tissue engineering, controlled release, and soil remediation. *Polymers* **2024**, 16, 2599.
18. Xie, X.F.; Lei, H.; Fan, D.D. Antibacterial hydrogel with pH-responsive microcarriers of slow-release VEGF for bacterial infected wounds repair. *J. Mater. Sci. Technol.* **2023**, 144, 198-212.
19. Faidi, A.; Lassoued, M.A.; Becheikh, M.E.H.; Touati, M.; Stumbé, J.-F.; Farhat, F. *A*pplication of sodium alginate extracted from a Tunisian brown algae Padina pavonica for essential oil encapsulation: Microspheres preparation, characterization and in vitro release study. *Int. J. Biol.* **2019**, 136, 386-394.
20. Han, Y.X.; Jiang, H.; Huang, C.; Wu, X.; Ouyang, Y.H.; Chen, H.F.; Lan, D.M.; Wang, Y.H.; Zheng, B.; Xia, J. Enzymatic interfacial conversion of acylglycerols in Pickering emulsions stabilized by hydrogel microparticles. *J. Colloid Interface Sci.* **2024**, 661, 228-236.
21. Ramdhan, T.; Ching, S.H.; Prakash, S.; Bhandari, B. Physical and mechanical properties of alginate based composite gels. *Trends Food Sci. Technol*. **2020**, 106, 150-159.
22. Ni, L.X.; Acharya, K.; Ren, G.X.; Li, S.Y.; Li, Y.P.; Li, Y. Preparation and characterization of anti-algal sustained-release granules and their inhibitory effects on algae. *Chemosphere* **2013**, 91, 608-615.
23. Zhu, L.Q.; Ouyang, F.F.; Fu, X.; Wang, Y.M.; Li, T.; Wen, M.; Zha, G.D.; Yang, X. Tannic acid modified keratin/sodium alginate/carboxymethyl chitosan biocomposite hydrogels with good mechanical properties and swelling behavior. *Sci. Rep*. **2024**, 14, 12864.
24. Wang, B.; Gao, B.; Wan, Y.S. Entrapment of ball-milled biochar in Ca-alginate beads for the removal of aqueous Cd (II). *J. Ind. Eng*. **2018**, 61, 161-168.
25. Guo, C.; Wu, S.J.; Gao, X.P.; Li, M.Y.; Long, H.M. Mechanistic study of Cr (VI) removal by modified alginate/GO composite via synergistic adsorption and photocatalytic reduction. *Int. J. Biol. Macromol*. **2021**, 189, 910-920.
26. Li, Y.H.; Liu, F.Q.; Xia, B.; Du, Q.J.; Zhang, P.; Wang, D.C.; Wang, Z.H.; Xia, Y.Z. Removal of copper from aqueous solution by carbon nanotube/calcium alginate composites. *J. Hazard. Mater*. **2010**, 177, 876-880.
27. He, D.D.; Zhang, Z.Y.; Zhang, W.B.; Zhang, H.; Liu, J.L. Municipal sludge biochar skeletal sodium alginate beads for phosphate removal. *Int. J. Biol. Macromol*. **2024**, 261, 129732.
28. Ahmed, A.S.; Alsultan, M.; Sabah, A.A.; Swiegers, G.F. Carbon dioxide adsorption by a high-surface-area activated charcoal. *J. Compos. Sci*. **2023**, 7, 179.
29. Huang, X.C.; Zhang, C.F.; Zhu, S.S.; Chen, D.; Ho, S.-H. Effects of biochar on microalgal growth: difference between dissolved and undissolved fractions. ACS Sustain. Chem. Eng. **2020**, 8, 9156-9164.

 doi:10.20944/preprints202604.2211.v1

30. Hussein, Y.H.; Tahseen, T.A.; Akroot, A.; Mithu, M.A.H.; Abdulateef, A.M. A multi-criteria optimization for a radial heat sink with semicircular fins based on the design of experiments approach. *Case Stud. Therm. Eng*. **2025**, 66, 105727.
31. Chong, B.W.; Shi, X.J. Meta-analysis on PET plastic as concrete aggregate using response surface methodology and regression analysis. *J. Infrastruct. Preserv. Resil*. **2023**, 4, 2.
32. Hu, L.; He, R.J.; Lu, Z.; Zhang, K.Q.; Bai, X.J. Step-freeze-drying method for carbon aerogels: a study of the effects on microstructure and mechanical property. *RSC Adv*. **2019**, 9, 9931-9936.
33. Su, H.Z.; Qiu, W.P.; Deng, T.R.; Zheng, X.L.; Wang, H.; Wen, P. Fabrication of physically multi-crosslinked sodium alginate/carboxylated-chitosan/montmorillonite-base aerogel modified by polyethyleneimine for the efficient adsorption of organic dye and Cu (II) contaminants. *Sep. Purif. Technol*. **2024,** 330, 125321.
34. Huang, B.Y.; Huang, D.; Zheng, Q.; Yan, C.H.; Feng, J.P.; Gao, H.J.; Fu, H.Q.; Liao, Y.W. Enhanced adsorption capacity of tetracycline on porous graphitic biochar with an ultra-large surface area. *RSC Adv*. **2023**, 13, 10397-10407.
35. Saito, K.; Xu, T.Y.; Ishikita, H. Correlation between C═O stretching vibrational frequency and p K a shift of carboxylic acids. *J. Phys. Chem. B*. **2022**, 126, 4999-5006.
36. Flores-Hernández, C.G.; Cornejo-Villegas, M.D.L.A.; Moreno-Martell, A.; Real, A.D. Synthesis of a Biodegradable Polymer of Poly (Sodium Alginate/Ethyl Acrylate). *Polymers* **2021**, 13, 504.
37. Hemzah, S.A.; Kurnia, I.; Eddy, D.R.; Rupaedah, B.; Suryana, S.; Bin Baz, A.; Ma'Amor, M.; Guan, G.Q.; Noviyanti, A.R. Hydrothermal synthesis of nanohydroxyapatite-activated carbon composites and its slow-release performance for urea. *Sci. Rep*. **2025**, 15, 26208.
38. Speranza, S.; Knechtl, R.; Witlaczil, R.; Schönlechner, R. Reversed-phase HPLC characterization and quantification and antioxidant capacity of the phenolic acids and flavonoids extracted from eight varieties of sorghum grown in Austria. *Front. Plant Sci.* **2021**, 12, 769151.
39. Liu, A.H.; Guo, H.; Ye, M.; Lin, Y.H.; Sun, J.H.; Xu, M.; Guo, D.A. Detection, characterization and identification of phenolic acids in Danshen using high-performance liquid chromatography with diode array detection and electrospray ionization mass spectrometry. *J. Chromatogr. A* **2007**, 1161, 170-182.
40. Rontani, J.F.; Galeron, M.A.; Auber, C. Electron ionization mass spectrometric fragmentation and multiple reaction monitoring quantification of ferulic and p-coumaric acid trimethylsilyl derivatives in deposited atmospheric particles. *Rapid Commun*. **2022**, 36, 9287.
41. Sinosaki, N.; Tonin, A.P.P.; Ribeiro, M.A.S.; Poliseli, C.B.; Roberto, S.B.; Silveira, R.d.; Visentainer, J.V.; Santos, O.O.; Meurer, E.C. Structural study of phenolic acids by triple quadrupole mass spectrometry with electrospray ionization in negative mode and H/D isotopic exchange. *J. Braz. Chem. Soc*. **2020**, 31, 402-408.
42. Ji, L.; Shi, W.J.; Li, Y.L.; He, J.; Xu, G.; Qin, M.; Guo, Y.Y.; Ma, Q. Systematic Identification, Fragmentation Pattern, And Metabolic Pathways of Hyperoside in Rat Plasma, Urine, And Feces by UPLC-Q-Exactive Orbitrap MS. *J. Anal. Methods Chem*. **2022**, 2022, 2623018.
43. van der Klift, E.; Villela, A.; Derksen, G.C.H.; Lankhorst, P.P.; van Beek, T.A. Microextraction of reseda luteola-dyed wool and qualitative analysis of its flavones by uhplc-uv, nmr and ms. *Molecules* **2021**, 26, 3787.
44. Lin, Y.X.; Li, T.J.; Zhang, Y.R. Effects of two typical quinolone antibiotics in the marine environment on Skeletonema costatum. *Front. Mar. Sci*. **2024**, 11, 1335582.
45. Huang, X.C.; Zhu, S.S.; Zhang, H.L.; Huang, Y.C.; Wang, X.D.; Wang, Y.; Chen, D. Biochar nanoparticles induced distinct biological effects on freshwater algae via oxidative stress, membrane damage, and nutrient depletion. *ACS Sustainable Chem. Eng*. **2021**, 9, 10761-10770.
46. Sun, L.; Zhang, L.Q.; Han, Q.; Feng, L. Prolonged Microcystis restraint through allelochemicals sustained-release microspheres regulated by carbon material (CM-AC@SM): Optimal formulation, characterization, effects and synergistic inhibition mechanisms. *Sci. Total Environ.* **2024**, 951, 175345.
47. Bustos, D.; Guzmán, L.; Valdés, O.; Muñoz-Vera, M.; Morales-Quintana, L.; Castro, R.I. Development and evaluation of cross-linked alginate–chitosan–abscisic acid blend gel. *Polymers* **2023**, 15, 3217.
48. Huang, D.J.; Ou, B.X.; Prior, R.L. The chemistry behind antioxidant capacity assays. *J. Agric. Food Chem.* **2005**, 53, 1841-1856.

 doi:10.20944/preprints202604.2211.v1

49. Wang, Y.J.; Wu, M.T.; Tang, P.Y.; Jiang, D.M. Chitosan/Sodium Alginate Hydrogel for the Release of Berberine as an Algae Suppressant: RSM Optimization and Analysis of Sustained Release Characteristics. *Gels* **2024**, 10, 591.
50. Chazaux, M.; Schiphorst, C.; Lazzari, G.; Caffarri, S. Precise estimation of chlorophyll a, b and carotenoid content by deconvolution of the absorption spectrum and new simultaneous equations for Chl determination. *Plant J.* **2022**, 109, 1630-1648.